

## Chapter 3

### Atomic Structure of ${}^9\text{Be}^+$ and Interaction with Lasers

If the Paul trap (spherical or elliptical) is the stage for our experiments, then it is the interaction of the ion(s) with light which sets the action in motion. Of course, atoms interacting with radiation are nothing new, but what is different with the experiments described herein is the well-controlled coupling between the ion's electronic degree of freedom and its motional degrees of freedom. This interaction is mediated by the field gradients inherent in the laser beams.

In this chapter, I will discuss the atomic structure of the  ${}^9\text{Be}^+$  ion in sufficient detail to understand our experiments. I will then go on to describe the interaction of the trapped ion with laser beams, and explain how this interaction couples the ion's electronic and motional degrees of freedom. In particular, I will focus in on two particular electronic levels, which I will describe in detail below. Note that the formalism used herein to describe the electronic degree of freedom relies heavily on the formal equivalence of a two-level system to a spin-1/2 particle. Indeed, I will use the terms "electronic degree of freedom" and "spin" interchangeably. For more on this topic, the reader is referred to Ref. [2].

The idea, then, is that our system presents us with two, basic quantum systems: the two-level system (formally equivalent to a spin-1/2 particle), and the quantum harmonic oscillator. Although these are two of the best-understood quantum systems, the coupling between them provides a wealth of interesting behaviour. A similar coupling,

and a similar wealth of behaviour, is found in cavity-QED systems [92], although there are differences between that system and the one described in this thesis.

### 3.1 Energy Levels of ${}^9\text{Be}^+$ and Single-Photon Transitions

Fig. 3.1 shows a simplified energy-level diagram for  ${}^9\text{Be}^+$ . The two-level system which is of interest to us is formed by two ground-state hyperfine levels: the  $2s\ 2S_{1/2}|F = 2, m_F = -2\rangle$  and  $2s\ 2S_{1/2}|F = 1, m_F = -1\rangle$  states, abbreviated by  $|\downarrow\rangle$  and  $|\uparrow\rangle$ , respectively.<sup>1</sup> These levels are separated by their hyperfine splitting. While running the experiment, we added a magnetic field of  $\approx 8$  Gauss, which further split the different  $m_F$  sub-levels of the  $F = 2$  and  $F = 1$  hyperfine levels, by  $\Delta E = g_F m_F \mu_B B$ . (Here,  $\mu_B \approx 1.4$  MHz/Gauss is the Bohr magneton,  $g_1 = -\frac{1}{2}$  and  $g_2 = +\frac{1}{2}$  are the Landé  $g$ -factors, and  $B$  is the magnitude of the magnetic field. The quantization axis determined by this magnetic field lay in the direction<sup>2</sup>  $-\frac{1}{\sqrt{2}}\mathbf{e}_x + \frac{1}{2}(\mathbf{e}_y - \mathbf{e}_z)$ . (Ambient magnetic fields such as that due to the Earth were nulled out using shim coils.) If we denote the total splitting of  $|\uparrow\rangle$  and  $|\downarrow\rangle$  by  $\omega_0$  then, in the course of the experiments, we had  $\omega_0/2\pi \approx 1.26$  GHz.

The  $2p\ 2P_{1/2}$  and  $2p\ 2P_{3/2}$  excited states are separated from the  $2s$  ground state by 313 nm. The fine-structure splitting between the  $2p$  levels is  $\approx 197$  GHz. The  $2P_{1/2}$  hyperfine splitting is  $\approx 237$  MHz, and the  $2P_{3/2}$  hyperfine splitting is less than 1 MHz. The natural linewidth of these states is  $\approx 19.4$  MHz.

When the ion is trapped in a strong harmonic potential, such as produced (in the pseudopotential approximation) by the ion trap, each of the electronic states is “dressed” with an associated “ladder” of motional eigenstates. In the diagram, I have only shown these motional states for  $|\downarrow\rangle$  and  $|\uparrow\rangle$ . In addition, for clarity and simplicity, I have

<sup>1</sup> Upon occasion, we used the  $2s\ 2S_{1/2}|F = 2, m_F = 2\rangle$  and  $|F = 1, m_F = 1\rangle$  states for the two level system. Aside from a slightly different energy separation between  $|\downarrow\rangle$  and  $|\uparrow\rangle$ , this had no significant effect upon the physics

<sup>2</sup> Note that, in this Chapter, I shall use the coordinate convention that the  $z$ -axis lies along the axis of symmetry of the coaxial resonator. The  $x$ - and  $y$ -axes lie along the other two principal directions of the trap. This is the convention used with the micromachined linear trap.

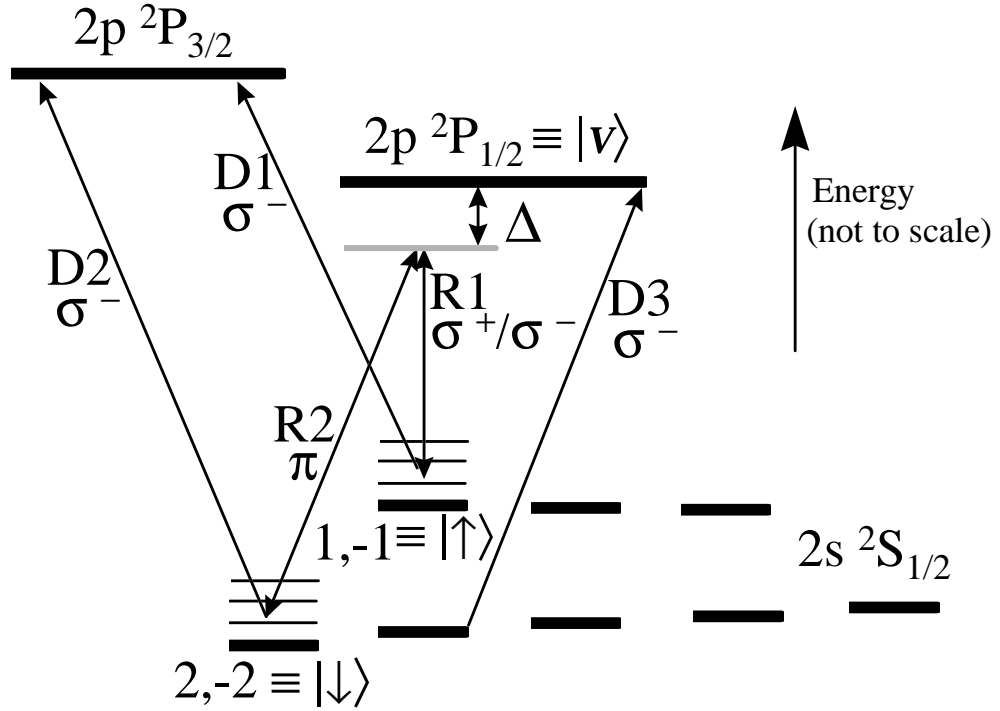


Figure 3.1: Simplified energy level diagram for  ${}^9\text{Be}^+$ , with energy increasing towards the top of the diagram (not to scale). The two levels of interest are the  $|F = 2, m_F = -2\rangle$  and  $|F = 1, m_F = -1\rangle$  hyperfine sub-levels (denoted  $|\downarrow\rangle$  and  $|\uparrow\rangle$ ) of the  $2s\ {}^2S_{1/2}$  ground state. The motional energy levels, spaced by  $\approx 10$  MHz, are indicated for these two states but are omitted for clarity in the other states. Single-photon transitions are driven by beams D1 and D2 to the  $2p\ {}^2P_{3/2}$  level (radiative linewidth  $\gamma/2\pi \approx 19.4$  MHz), and  $|\downarrow\rangle$  and  $|\uparrow\rangle$  are coupled through the  $2p\ {}^2P_{1/2}$  level using two-photon, stimulated Raman transitions driven by beams R1 and R2 ( $\Delta/2\pi \approx 40$  GHz). Beam D3 clears population out of the  $2s\ {}^2S_{1/2}|F = 2, m_F = -1\rangle$  level. These optical transitions correspond to a laser wavelength of 313 nm. For further details, see Ch. 3. The  ${}^2S_{1/2}$  hyperfine splitting is  $\omega_0/2\pi \approx 1.25$  GHz, the  ${}^2P$  fine-structure splitting is  $\approx 197$  GHz, the  ${}^2P_{1/2}$  hyperfine splitting is  $\approx 237$  MHz, and the  ${}^2P_{3/2}$  hyperfine structure ( $< 1$  MHz) is unresolved. The Zeeman splitting between adjacent  $m_F$  levels is  $\approx 0.7$  MHz/Gauss. Under typical operating conditions, the Zeeman contribution to the  $|\downarrow\rangle - |\uparrow\rangle$  splitting was about 12 MHz.

indicated only the motional eigenstates associated with a single direction  $m$  ( $m = x, y,$  or  $z$ ). These states are spaced by energy  $\hbar\omega_m$ .

One may use an ultraviolet laser beam with  $\lambda \approx 313$  nm to couple either  $|\uparrow\rangle$  or  $|\downarrow\rangle$  to the  $2p^2P_{3/2}$  excited electronic state. In particular, the transition  $|\downarrow\rangle \rightarrow |2p^2P_{1/2}, F = 3, m_F = -3\rangle$  is a cycling transition (driven by laser beam D2). Thus, if the atom is in  $|\downarrow\rangle$  and the laser light is polarized  $\sigma^+$ , then the atom repeatedly cycles between this state and the excited state  $|F = 3, m_F = -3\rangle$ , spontaneously emitting a photon each time. It repeats this cycle until slight imperfections in the laser polarization cause transitions to a different excited state, from which the atom can decay to a different ground-state level where the laser is off-resonant. Thus, this transition allows determination of whether the ion is in the state  $|\downarrow\rangle$  (and, by inference,  $|\uparrow\rangle$ ) with almost unit quantum efficiency [56, 57, 58].

On the other hand, the transition  $|\uparrow\rangle \rightarrow |2p^2P_{1/2}, F = 3, m_F = -2\rangle$ , which is driven by beam D1, is not a cycling transition. From the excited state, the atom can decay back to  $|\uparrow\rangle$ , to  $|\downarrow\rangle$ , or to the  $|2s^2S_{1/2}, F = 2, m_F = -1\rangle$  state. In the latter case, we have to re-pump the atom back into the two-level system. In practice, we did this with laser beam D3, resonant with the  $|2s^2S_{1/2}, F = 2, m_F = -1\rangle \rightarrow |2p^2P_{1/2}, F = 2, m_F = -2\rangle$  transition, which optically pumped the ion back into the  $|\uparrow\rangle/|\downarrow\rangle$  manifold. When D2 and D3 were turned on together, the ion was optically pumped into  $|\downarrow\rangle$ . This optical pumping was used to initialize the spin state of the ion at the beginning of each experiment.

Returning to state detection with the cycling transition, Fig. 3.2 shows histograms of the number of photon counts measured per experiment with the ion in  $|\downarrow\rangle$  and in  $|\uparrow\rangle$ .<sup>3</sup> In practice, several factors limited the quantum efficiency of spin detection. Since the hyperfine splitting in the  $2p^2P_{3/2}$  level is negligible, the efficiency of the cycling transition is, in part, determined by the degree to which beam D2 is pure  $\sigma^+$ .

---

<sup>3</sup>  $|\uparrow\rangle$  is prepared from  $|\downarrow\rangle$  using a  $\pi$ -pulse Raman transition (see next Section)

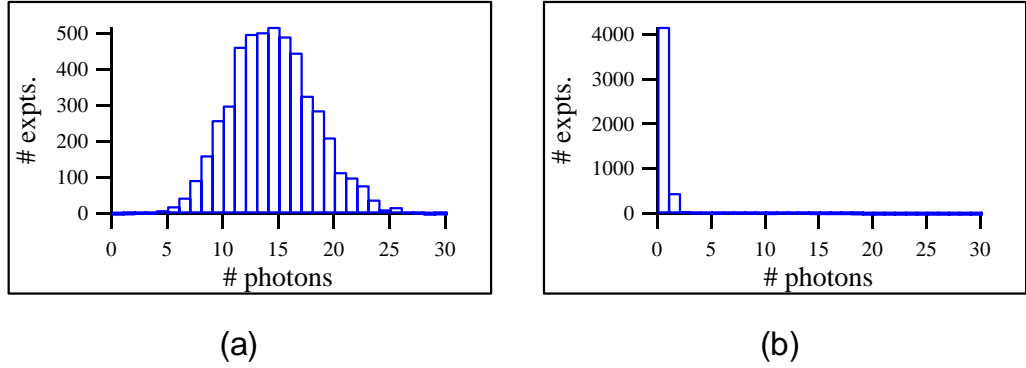


Figure 3.2: (a) Photon number histogram on the cycling transition when the ion starts out in the state  $|\downarrow\rangle$ . (b) Photon number histogram for the state  $|\uparrow\rangle$ . The counts in channels one and two are due to background and to off-resonant pumping out of  $|\uparrow\rangle$  by the cycling transition beam (see Appendix A).

The quantum efficiency of the  $|\uparrow\rangle/|\downarrow\rangle$  determination is also fundamentally limited by the atomic physics of  ${}^9\text{Be}^+$ : since the ground-state hyperfine splitting is only about 60 times the excited state linewidth, spontaneous emission after off-resonant transitions from  $|\uparrow\rangle$  to the excited state can transfer population from  $|\uparrow\rangle$  into the cycling transition. For a given effective quantum efficiency of the photodetection system (solid angle and photodetection quantum efficiency), this places a limit on the quantum efficiency of  $|\uparrow\rangle/|\downarrow\rangle$  discrimination. For our typical operating conditions, this discrimination quantum efficiency was 96-98%. For a more complete discussion of this effect, and a discussion of other uses of the photon number histograms, see Appendix A.

### 3.2 Coupling Spin and Motion

Single-photon transitions are thus useful for optical pumping and for detecting which of the states ( $|\downarrow\rangle$  or  $|\uparrow\rangle$ ) the atom is in. However, we still need a way to couple the ion's electronic levels *coherently* to its motion if we wish to produce quantum entanglement between the spin and motion, or to use entangle the spins of separate ions using their collective motion as an intermediary. Such a coupling must be spectrally

narrow enough to resolve different states of ionic motion. Furthermore, in order to couple the ion's electronic state with its motion, we require strong field gradients.

To see how this coupling occurs, first consider the Hamiltonian of a single, trapped ion interacting with an applied electric field in the case when two of its levels (which I will denote  $\downarrow$  and  $\uparrow$ ) have an allowed electric dipole transition between them:<sup>4</sup>

$$\hat{H} = \hat{H}_{\uparrow\downarrow} + \hat{H}_{HO} + \hat{H}_{int}. \quad (3.1)$$

Here,  $\hat{H}_{\uparrow\downarrow} = \frac{1}{2}\hbar\omega_0\hat{\sigma}_3$  is the free Hamiltonian for the two-level system  $\{|\uparrow\rangle, |\downarrow\rangle\}$  and, in the usual spin- $\frac{1}{2}$  formalism,  $\hat{\sigma}_3$  is the Pauli spin operator.<sup>5</sup>  $\hat{H}_{HO} = \hbar\hat{\mathbf{n}} \cdot \boldsymbol{\omega}$  is the Hamiltonian for motion along the  $x$ -direction, with  $\hat{\mathbf{n}} = (\hat{n}_x, \hat{n}_y, \hat{n}_z)$ , ( $\hat{n}_m$  being the number operator for direction  $m$ ),  $\boldsymbol{\omega} = (\omega_x, \omega_y, \omega_z)$ , and the zero-point energy suppressed.

Finally,

$$\hat{H}_{int} = -\hat{\boldsymbol{\mu}} \cdot \mathbf{E}(\hat{\mathbf{x}}, t) \quad (3.2)$$

expresses the interaction between the ion and the laser beams, in the electric-dipole approximation [93]. In Eq. 3.2,  $\hat{\boldsymbol{\mu}} = e\mathbf{r}_{el}$  is the electric dipole moment of the atom (with  $\mathbf{r}_{el}$  the electron-nucleus relative position operator) and  $\hat{\mathbf{x}}$  is the position operator for the ion's centre- of-mass. This dependence of  $\hat{H}_{int}$  on the ion's position gives the desired coupling between the ion's motional and spin degrees of freedom. For example, suppose that  $\mathbf{E} = E(\hat{z}, t)\mathbf{e}_x$  (where  $\mathbf{e}_x$  is the unit vector in the  $x$ -direction). If we expand the electric field in a power series, we have that

$$\hat{H}_{int} = -\hat{\mu}_x \left[ E(z=0, t) + \frac{\partial E}{\partial z} \Big|_{z=0} \hat{z} + \frac{\partial^2 E}{\partial z^2} \Big|_{z=0} \hat{z}^2 + \dots \right]. \quad (3.3)$$

The key term in Eq. (3.3) is the gradient term. Suppose, for instance, that the electric field were constant in time, but spatially non-uniform. Since the ion is oscillating in

---

<sup>4</sup> The  ${}^9\text{Be}^+$  ground state hyperfine levels which I identified as  $\downarrow$  and  $\uparrow$  above do not have such a transition. However, they may be coupled by two-photon, stimulated Raman transitions, which I will discuss in Sec. 3.3.

<sup>5</sup> Another notation for the Pauli operators uses  $\hat{\sigma}_x \equiv \hat{\sigma}_1$ ,  $\hat{\sigma}_y \equiv \hat{\sigma}_2$ , and  $\hat{\sigma}_z \equiv \hat{\sigma}_3$ . However, to avoid confusion with the motional operators, I will use the present notation. The Pauli operators act in the Hilbert space of the ion's spin degree of freedom.

the  $z$ -direction, it experiences a modulation of  $\mathbf{E}$  at the ion's oscillation frequency (in the rest frame of the ion). So, if the oscillation frequency were equal to the atomic transition frequency  $\omega_0$ , the static field could still cause transitions between electronic levels.

In practice, time-dependent fields are used to drive transitions. However, the idea remains the same: field gradients couple the spin and motion and drive transitions. To flesh this out a bit, consider the one-dimensional case of a single ion constrained to move only in the  $z$ -direction, interacting with an electric field  $\mathbf{E}(z, t) = E_0 \mathbf{e}_x \cos(kz - \omega_L t + \phi)$ . For the following derivation, I shall assume that the laser linewidth is much less than the motional frequency, so that the different motional sidebands are spectrally resolved. This is the so-called “resolved-sideband” regime.

The interaction Hamiltonian for such a situation is given by

$$\hat{H}_{int} = \hbar\Omega(\hat{S}_+ + \hat{S}_-)(e^{i(k\hat{z} - \omega_L t + \phi)} + e^{-i(k\hat{z} - \omega_L t + \phi)}), \quad (3.4)$$

where  $\hat{\Omega} \doteq -\hat{\mu}E_0/2$  is the Rabi frequency, giving the interaction strength between the ion and the field, and  $\hat{S}_\pm = \hbar(\hat{\sigma}_1 \pm i\hat{\sigma}_2)/2$  are the atomic raising and lowering operators which indicate the effect of the interaction on the atomic levels  $|\downarrow\rangle$  and  $|\uparrow\rangle$ . Now let us go into an interaction picture defined by  $\hat{H}_0 = \hat{H}_{\uparrow\downarrow} + \hat{H}_{HO}$  and  $\hat{V}_{interaction} = \hat{H}_{int}$ . Then

$$\begin{aligned} \hat{H}'_{int} &= \hbar\Omega(\hat{S}_+ e^{i\omega_0 t} + \hat{S}_- e^{-i\omega_0 t}) \left[ \exp(i[\eta(\hat{a}e^{-i\omega_z t} + \hat{a}^\dagger e^{i\omega_z t})]) e^{-i(\omega_L t + \phi)} \right. \\ &\quad \left. + \exp(-i[\eta(\hat{a}e^{-i\omega_z t} + \hat{a}^\dagger e^{i\omega_z t})]) e^{i(\omega_L t - \phi)} \right]. \end{aligned} \quad (3.5)$$

In this last equation, I have expressed  $\hat{z} = z_0(\hat{a} + \hat{a}^\dagger)$ , where  $z_0 = \sqrt{\frac{\hbar}{2m\omega_z}}$  is the spread of the ground state harmonic oscillator wave function ( $\psi_0(z) = (\frac{m\omega_z}{\pi\hbar})^{1/4} \exp[-m\omega_z z^2/2\hbar]$ ), and then defined the Lamb-Dicke parameter:  $\eta \doteq k_z z_0$ .

Now, I will make the “rotating wave” approximation: assuming that  $\omega_L \approx \omega_0$ , I will drop terms which have an exponent oscillating at optical frequencies. The idea

behind this is that such terms will average to zero on the long (compared to optical time scales) time scales of interest to us.<sup>6</sup> Defining the detuning  $\delta = \omega_L - \omega_0$  of the laser from resonance, we have:

$$\hat{H}'_{int} = \hbar\Omega \left[ S_+ \exp \left( i\eta (a_z^\dagger e^{i\omega_z t} + a_z e^{-i\omega_z t}) - i\delta t + i\phi \right) \right] + H.C. \quad (3.6)$$

We may expand the first term in the exponential in Eq. 3.6 in a power series in  $\eta$  to obtain

$$\hat{H}'_{int} = \hbar\Omega \left[ S_+ \sum_{k=0}^{\infty} \frac{(i\eta)^k (a_z^\dagger e^{i\omega_z t} + a_z e^{-i\omega_z t})^k}{k!} \right] e^{-i(\delta t - \phi)} + H.C. \quad (3.7)$$

At this point, if we make one final rotating-wave approximation, it may be apparent that the detuning  $\delta$  picks out different powers of  $a$ ,  $a^\dagger$ : that is, depending on  $\delta$ , different motional levels are coupled together.

Going back to the general expression, Eq. (3.7), we can put  $\hat{H}'_{int}$  into the Schrödinger equation for the interaction-picture state vector. Since I will assume that we are close to one of the resonances implicit in Eq. (3.6), let  $\delta = (n - m)\omega_z + \epsilon$ , where  $|\epsilon| \ll \omega_z, \Omega$  and  $n, m$  are the indices of the motional levels coupled by the resonance. Representing  $|\Psi\rangle = \sum_{\{j=\uparrow, \downarrow\}} \sum_n C'_{j,n}(t) |j, n\rangle$ , we obtain:

$$\dot{C}'_{\uparrow, n} = -i^{(1+|n-m|)} e^{-i(\epsilon t - \phi)} \Omega_{n,m} C'_{\downarrow, m} \quad (3.8)$$

$$\dot{C}'_{\downarrow, m} = -i^{(1-|n-m|)} e^{i(\epsilon t - \phi)} \Omega_{n,m} C'_{\uparrow, n}. \quad (3.9)$$

In these equations,

$$\Omega_{n,m} = \Omega \langle n | e^{i\eta(\hat{a}_z + \hat{a}_z^\dagger)} | m \rangle \quad (3.10)$$

is the Rabi frequency for the coupling between levels  $|\uparrow, n\rangle$  and  $|\downarrow, m\rangle$ . Another way to express  $\Omega_{n,m}$  is:

$$\Omega_{n,m} = \Omega \langle n | \hat{D}(i\eta) | m \rangle, \quad (3.11)$$

---

<sup>6</sup> Note that these terms have very large energy denominators in a perturbative expansion and, thus, are indeed negligible

where  $\hat{D}(\alpha) = e^{\alpha\hat{a}^\dagger - \alpha^*\hat{a}}$  is the displacement operator [94]. We may evaluate the expectation value in Eq. (3.27) to obtain:

$$\Omega_{n,m} = \Omega e^{-\eta^2/2} \sqrt{\frac{n_{<}!}{n_{>}!}} \eta^{|m-n|} L_{n_{<}}^{|m-n|}(\eta^2), \quad (3.12)$$

where  $L_n^m$  is an associated Laguerre polynomial [72, 94]. In the Lamb-Dicke limit,  $\eta \ll 1$ , this expression simplifies considerably and, for example, we have that  $\Omega_{n,n-1} = \eta\Omega\sqrt{n}$ , and that  $\Omega_{n,n+1} = \eta\Omega\sqrt{n+1}$ .

The dynamics described by Eq. (3.9) exhibit Rabi oscillations between  $|\uparrow, n\rangle$  and  $|\downarrow, m\rangle$ . In particular, if we express  $|\Psi\rangle$  as a column vector,  $|\Psi\rangle \equiv \begin{bmatrix} C_{\uparrow,n} \\ C_{\downarrow,m} \end{bmatrix}$ , then we have

$$\begin{aligned} |\Psi(t)\rangle = & \\ & \begin{bmatrix} e^{-i\epsilon t/2} [\cos(\frac{X_{n,m}t}{2}) + i\frac{\epsilon}{X_{n,m}} \sin(\frac{X_{n,m}t}{2})] & -2i\frac{\Omega_{n,m}}{X_{n,m}} e^{-i(\epsilon t - 2\phi - \pi|m-n|)/2} \sin(\frac{X_{n,m}t}{2}) \\ -2i\frac{\Omega_{n,m}}{X_{n,m}} e^{i(\epsilon t - 2\phi - \pi|m-n|)/2} \sin(\frac{X_{n,m}t}{2}) & e^{i\epsilon t/2} [\cos(\frac{X_{n,m}t}{2}) - i\frac{\epsilon}{X_{n,m}} \sin(\frac{X_{n,m}t}{2})] \end{bmatrix} \\ & \times |\Psi(0)\rangle, \end{aligned} \quad (3.13)$$

where  $X_{n,m} = \sqrt{\epsilon^2 + 4\Omega_{n,m}^2}$ . On resonance,  $\epsilon = 0$ , Eq. (3.13) simplifies to:

$$|\Psi(t)\rangle = \begin{bmatrix} \cos(\Omega_{n,m}t) & -ie^{i(\phi+\pi|m-n|/2)} \sin(\Omega_{n,m}t) \\ -ie^{-i(\phi+\pi|m-n|/2)} \sin(\Omega_{n,m}t) & \cos(\Omega_{n,m}t) \end{bmatrix} |\Psi(0)\rangle, \quad (3.14)$$

which indicates sinusoidal oscillations between  $|\downarrow, n\rangle$  and  $|\uparrow, m\rangle$ .

To put all this on a more physical footing, suppose that we prepare the atom in  $|\downarrow\rangle$  through optical pumping and turn on the laser interaction for some time  $t_{pr}$ , then measure the occupation of the state  $|\downarrow\rangle$  through the cycling transition. If we repeat this process for various relative detunings  $\delta$  of the laser, we build up a spectrum of the form shown in Fig. 3.3.

The central feature in Fig. 3.3 is the so-called ‘‘carrier’’ transition at  $\delta = 0$ . This transition couples the levels  $|\downarrow, n\rangle \leftrightarrow |\uparrow, n\rangle$ ; that is, it flips the spin but leaves the ion’s motional state unaffected. If we sit on resonance,  $\delta = 0$ , and apply the interaction for time  $t_{pr}$ , then the probability  $P_{\downarrow}$  is (in the Lamb-Dicke limit) given by

$$P_{\downarrow}(t_{pr}) = \cos^2(\Omega t_{pr}). \quad (3.15)$$

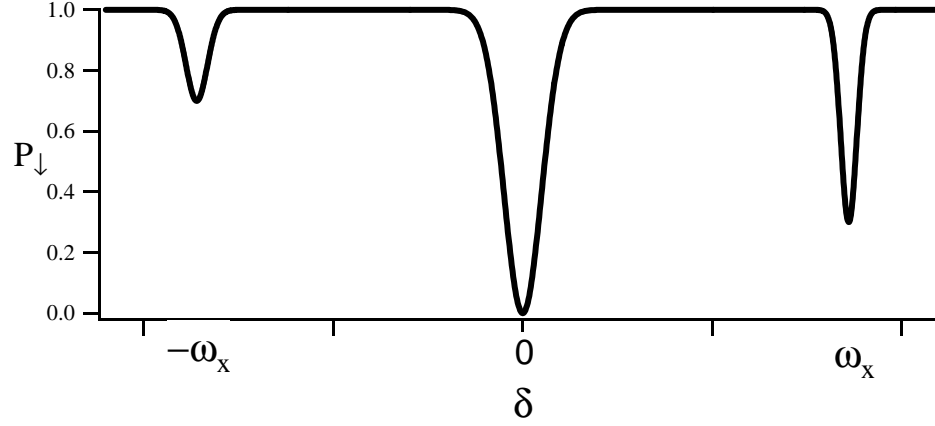


Figure 3.3: Representation of the spectrum swept out when the Raman laser beam difference frequency  $\delta + \omega_0$  is swept, holding the length of the probe pulse constant ( $\Omega t_{pr} = \pi/2$ ). The signal we measure is proportional to the probability that the ion remains in  $|\downarrow\rangle$  after the probe pulse. The feature at  $\delta = 0$  is the carrier, which flips the ion spin but does not affect the motion. The upper motional (or “blue”) sideband, at  $\delta = +\omega_x$  couples the levels  $|\downarrow, n\rangle \leftrightarrow |\uparrow, n+1\rangle$ . The lower (or “red”) sideband, at  $\delta = -\omega_x$  couples  $|\downarrow, n\rangle \leftrightarrow |\uparrow, n-1\rangle$ , and vanishes if the ion starts out in  $|\downarrow, n=0\rangle$ .

This sort of behaviour is indicated by the “Rabi flopping curve” in Fig. 3.4(a). In the usual nomenclature, a pulse for which  $\Omega t_{pr} = \pi/2$ , and thus for which the population is inverted (since  $P_{\downarrow}$  oscillates at  $2\Omega$ ) is referred to as a “ $\pi$  pulse.” One for which  $\Omega t_{pr} = \pi$  is referred to as a “ $2\pi$  pulse,” and so on.

The feature at  $\delta = +\omega_x$  in Fig. 3.3 is the first upper motional (or “blue”) sideband, which couples the levels  $|\downarrow, n\rangle \leftrightarrow |\uparrow, n+1\rangle$ . In this case, the ion undergoes Rabi flopping between these two levels with Rabi frequency  $\Omega_{n,n+1}$ . In the Lamb-Dicke regime  $\Omega_{n,n+1} = \eta\Omega\sqrt{n+1}$ . However, outside the Lamb-Dicke regime contributions to the Rabi frequency from higher-order terms in the sum of Eq. (3.7) with equal powers of  $a$  and  $a^\dagger$  also contribute to the Rabi frequency, and we must use the general expression,

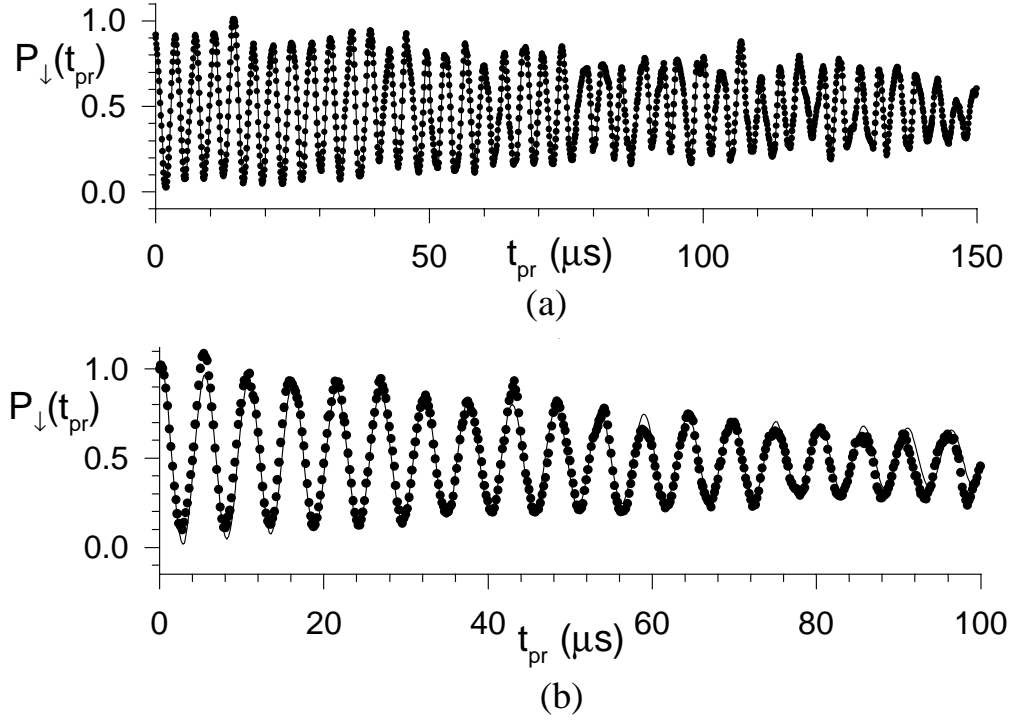


Figure 3.4: (a) “Rabi flopping curve” showing the ground-state occupation probability  $P_{\downarrow}(t_{pr})$  for the carrier transition:  $\delta = 0$  (see Eq. 3.15). Each point represents an average of  $\approx 4000$  measurements, or 1 s of integration. The slow decay of the envelope is mostly due to technical noise, with small contributions due to background heating of the ion’s motion (which affects the single-photon carrier Rabi frequency at order  $\eta^2$ ). (b) Ground state occupation probability  $P_{\downarrow}(t_{pr})$  for the first upper (“blue”) sideband:  $\delta = +\omega_x$ , starting in the ground state. The envelope decay is due to both technical noise and some background heating of the ion’s motion.

Eq. (3.12). A typical upper (“blue”) sideband Rabi flopping curve for a harmonic-oscillator motional eigenstate is shown in Fig. 3.4(b).

Finally, the feature at  $\delta = -\omega_z$  in Fig. 3.3 is the first lower (or “red”) sideband, coupling  $|\downarrow, n\rangle \leftrightarrow |\uparrow, n-1\rangle$ . Thus, if the ion starts out in the motional state  $|\downarrow, n=0\rangle$ , this feature vanishes (since there is no lower vibrational state with which to couple). The Rabi frequency on the lower sideband is  $\Omega_{n,n-1} = \Omega\eta\sqrt{\frac{1}{n}}e^{-\eta^2/2}L_{n-1}^1(\eta^2)$  (or  $\Omega_{n,n-1} = 0$  if the ion is in its ground state), which, in the Lamb-Dicke regime, reduces to  $\Omega_{n,n-1} =$

$\eta\sqrt{n}\Omega$ . In this regime, the interaction Hamiltonian for the trapped ion interacting with the laser beam is formally equivalent to the Hamiltonian of Cavity-QED [92].

It is worth noting that one can treat the interaction between the lasers and the ion's complete motion (including the micromotion) in a completely quantum-mechanical manner [70]. However, such a treatment does not alter any of the results significantly. Although this treatment does show that one can perform, for example, laser cooling on rf-sidebands (i.e. sidebands induced by the ion's micromotion), we shall see in Sec. 6.4.1, we can predict much of the relevant behaviour by treating the micromotion as classical, as indicated in Ch. 2.

### 3.3 Two-Photon, Stimulated-Raman Transitions

Rather than use single-photon transitions to couple  $|\downarrow\rangle$  ( $|F = 2, m_F = -2\rangle$ ) and  $|\uparrow\rangle$  ( $|F = 1, m_F = -1\rangle$ ) in our experiment, we use two-photon, stimulated Raman transitions. That is, we apply two laser beams with  $\Delta\omega_L = \omega_{L1} - \omega_{L2} = \omega_0 + \delta$  and  $\Delta\mathbf{k} = \mathbf{k}_1 - \mathbf{k}_2$ . Each laser beam is detuned by  $\Delta_R$  from resonance with the  $2p^2P_{1/2}$  level. The result is that transitions are driven from  $|\downarrow\rangle$  to  $|\uparrow\rangle$ , with the  $2p^2P_{1/2}$  level serving as a “virtual level” (which I will refer to as  $|v\rangle$ ). The difference frequency between the two Raman beams is determined by a radio frequency, with its associated low level of frequency jitter. At the same time, by choosing  $\Delta\mathbf{k}$  judiciously, we have the high field gradients (e.g.  $\frac{\partial\mathbf{E}}{\partial z} \propto k_z\mathbf{E}$ ) associated with optical wavelengths. Using Raman transitions also allows us to be selective in coupling the spin and the motion. In general, these transitions are sensitive to motion in all three principal trap directions. But, for example, if  $\Delta\mathbf{k} \parallel \mathbf{e}_z$ , we are only sensitive to motion in the  $z$ -direction, and if  $\Delta\mathbf{k} \approx 0$ , we are highly insensitive to motion.

To quantify the situation, let  $\mathbf{E}_1(\mathbf{x}, t) = \epsilon_1 E_1 \cos(\mathbf{k}_1 \cdot \mathbf{r} - \omega_{L1}t + \phi_1)$  and  $\mathbf{E}_2(\mathbf{x}, t) = \epsilon_2 E_2 \cos(\mathbf{k}_2 \cdot \mathbf{r} - \omega_{L2}t + \phi_2)$  (where  $\epsilon_j$  gives the polarization of the  $j^{\text{th}}$  laser). Then the

interaction Hamiltonian may be written as:

$$H_{int} = -\hbar \left[ \hat{g}_1^\dagger e^{i\mathbf{k}_1 \cdot \hat{\mathbf{x}}} e^{i\omega_{L1}t} + \hat{g}_2^\dagger e^{i\mathbf{k}_2 \cdot \hat{\mathbf{x}}} e^{i\omega_{L2}t} + H.C. \right], \quad (3.16)$$

where  $\hat{g}_i = E_i e^{-i\phi_i} \boldsymbol{\epsilon}_i \cdot \hat{\mathbf{x}} / 2\hbar$  ( $i = 1, 2$ ) and  $e$  is the charge of the electron.

Let  $C_{j,\mathbf{n}} = \langle j, \mathbf{n} | \psi \rangle$ , where  $j \in \{\uparrow, \downarrow, v\}$  and  $|\psi\rangle$  is the state of the system. If we go into an interaction picture defined by  $\hat{H}_0 = \hat{H}_{elec} + \hat{H}_{HO}$  (where  $\hat{H}_{elec}$  includes contributions from  $H_{\uparrow\downarrow}$  and the energy of the level  $|v\rangle$ ), and  $\hat{V}_{interaction} = \hat{H}_{int}$ , then we find that

$$\dot{C}'_{\downarrow,\mathbf{n}} = ig_1^* \sum_{\mathbf{n}'} \langle \mathbf{n} | e^{-i\mathbf{k}_1 \cdot \hat{\mathbf{x}}} | \mathbf{n}' \rangle e^{i[\boldsymbol{\omega} \cdot (\mathbf{n} - \mathbf{n}') - \Delta_R]t} C'_{v,\mathbf{n}'} \quad (3.17)$$

$$\dot{C}'_{\uparrow,\mathbf{n}} = ig_2^* \sum_{\mathbf{n}'} \langle \mathbf{n} | e^{-i\mathbf{k}_2 \cdot \hat{\mathbf{x}}} | \mathbf{n}' \rangle e^{i[\boldsymbol{\omega} \cdot (\mathbf{n} - \mathbf{n}') - \Delta_R - \delta]t} C'_{v,\mathbf{n}'} \quad (3.18)$$

$$\begin{aligned} \dot{C}'_{v,\mathbf{n}} &= ig_1 \sum_{\mathbf{n}'} \langle \mathbf{n} | e^{i\mathbf{k}_1 \cdot \hat{\mathbf{x}}} | \mathbf{n}' \rangle e^{i[\boldsymbol{\omega} \cdot (\mathbf{n} - \mathbf{n}') + \Delta_R]t} C'_{\downarrow,\mathbf{n}'} + \\ &\quad ig_2 \sum_{\mathbf{n}'} \langle \mathbf{n} | e^{i\mathbf{k}_2 \cdot \hat{\mathbf{x}}} | \mathbf{n}' \rangle e^{i[\boldsymbol{\omega} \cdot (\mathbf{n} - \mathbf{n}') + \Delta_R + \delta]t} C'_{\uparrow,\mathbf{n}'}. \end{aligned} \quad (3.19)$$

Here,  $g_1 \doteq \langle \downarrow | \hat{g}_1 | v \rangle$ ,  $g_2 \doteq \langle \uparrow | \hat{g}_2 | v \rangle$ , and the  $C'_{i,\mathbf{n}}$  are the coefficients of the interaction-picture state vectors. In writing these three equations, I have made the ‘‘rotating wave approximation:’’ that is, I have neglected terms with time-dependences at optical frequencies. If we now make the substitution  $\tilde{C}_{v,\mathbf{n}} \doteq C_{v,\mathbf{n}} e^{-i\Delta_R t}$  (corresponding to a transformation to a new interaction picture), we obtain:

$$\dot{\tilde{C}}'_{\downarrow,\mathbf{n}} = ig_1^* \sum_{\mathbf{m}} \langle \mathbf{n} | e^{-i\mathbf{k}_1 \cdot \hat{\mathbf{x}}} | \mathbf{m} \rangle e^{i[\boldsymbol{\omega} \cdot (\mathbf{n} - \mathbf{m})]t} \tilde{C}'_{v,\mathbf{m}} \quad (3.20)$$

$$\dot{\tilde{C}}'_{\uparrow,\mathbf{n}} = ig_2^* \sum_{\mathbf{m}} \langle \mathbf{n} | e^{-i\mathbf{k}_2 \cdot \hat{\mathbf{x}}} | \mathbf{m} \rangle e^{i[\boldsymbol{\omega} \cdot (\mathbf{n} - \mathbf{m}) - \delta]t} \tilde{C}'_{v,\mathbf{m}} \quad (3.21)$$

$$\begin{aligned} \dot{\tilde{C}}'_{v,\mathbf{n}} + i\Delta \tilde{C}'_{v,\mathbf{n}} &= ig_1 \sum_{\mathbf{m}} \langle \mathbf{n} | e^{i\mathbf{k}_1 \cdot \hat{\mathbf{x}}} | \mathbf{m} \rangle e^{i[\boldsymbol{\omega} \cdot (\mathbf{n} - \mathbf{m})]t} \tilde{C}'_{\downarrow,\mathbf{m}} + \\ &\quad ig_2 \sum_{\mathbf{m}} \langle \mathbf{n} | e^{i\mathbf{k}_2 \cdot \hat{\mathbf{x}}} | \mathbf{m} \rangle e^{i[\boldsymbol{\omega} \cdot (\mathbf{n} - \mathbf{m}) + \delta]t} \tilde{C}'_{\uparrow,\mathbf{m}}. \end{aligned} \quad (3.22)$$

At this point, we perform an adiabatic elimination of the excited state  $|v\rangle$ : we assume  $\dot{\tilde{C}}'_{v,\mathbf{n}} \ll i\Delta \tilde{C}'_{v,\mathbf{n}}$  and solve the last of the three equations above for  $\tilde{C}'_{3,\mathbf{n}}$ . Plugging this into the first two equations, we obtain:

$$\dot{C}'_{\downarrow,\mathbf{n}} = i \frac{|g_1|^2}{\Delta_R} C'_{\downarrow,\mathbf{n}} + i \frac{g_1^* g_2}{\Delta_R} \sum_{\mathbf{m}} \langle \mathbf{n} | e^{-i\boldsymbol{\Delta} \mathbf{k} \cdot \hat{\mathbf{x}}} | \mathbf{m} \rangle e^{i[\boldsymbol{\omega} \cdot (\mathbf{n} - \mathbf{m}) + \delta]t} C'_{\uparrow,\mathbf{m}} \quad (3.23)$$

$$\dot{C}'_{\uparrow,\mathbf{n}} = i\frac{|g_2|^2}{\Delta}C'_{\uparrow,\mathbf{n}} + i\frac{g_2^*g_1}{\Delta_R}\sum_{\mathbf{m}}\langle\mathbf{n}|e^{i\Delta\mathbf{k}\cdot\hat{\mathbf{x}}}|m\rangle e^{i[\boldsymbol{\omega}\cdot(\mathbf{n}-\mathbf{m})-\delta]t}C'_{\downarrow,\mathbf{m}}. \quad (3.24)$$

with  $\Delta\mathbf{k} = \mathbf{k}_1 - \mathbf{k}_2$ . The first terms in these equations,  $i|g_j|^2/\Delta_R$ , represent AC Stark shifts of  $|\uparrow\rangle$  and  $|\downarrow\rangle$ . These can be eliminated from our discussion by redefining the energies of  $|\uparrow\rangle$  and  $|\downarrow\rangle$  to include them, or by transforming to yet another interaction picture. The interesting dynamics are induced by the second terms in the equations.

The expressions  $\langle\mathbf{n}|e^{i\Delta\mathbf{k}\cdot\hat{\mathbf{x}}}|m\rangle$  determine the strength of the coupling between the different motional levels. For example, if  $\Delta\mathbf{k} = \mathbf{0}$ , then only levels for which  $\mathbf{m} = \mathbf{n}$  are coupled; that is, the interaction with the lasers changes the spin state but *not* the motional state, as claimed above. Moreover, in contrast to Eq. (3.12), the  $|\downarrow\rangle \leftrightarrow |\uparrow\rangle$  carrier Rabi frequency is independent of the motional state. If  $\Delta\mathbf{k} \parallel \mathbf{e}_z$ , then the coupling is sensitive to motion only in the  $z$ -direction, and only different  $z$ -motional states are coupled; in this case, the sums collapse down to one-dimensional ones (i.e. sums over  $n_z$ ).

The detuning  $\delta$  picks out particular terms in the sums. For example, assume, that  $\Delta\mathbf{k} \parallel \mathbf{e}_z$  so that  $\Delta\mathbf{k} = k_z\hat{z}$ , and assume that  $\delta \approx \omega_z(n_z - m_z)$  for some particular  $n_z - m_z$ . Then this term will be slowly-varying with respect to all the other terms in the sum, and another rotating-wave approximation allows us to drop all these other terms (which average to zero). Then Eqs. (3.24) become:

$$\dot{C}'_{\downarrow,n_z} = -i\Omega_{n,m}^*e^{i\delta t}C'_{\uparrow,m} \quad (3.25)$$

$$\dot{C}'_{\uparrow,n_z} = -i\Omega_{n,m}e^{-i\delta t}C'_{\downarrow,m}. \quad (3.26)$$

Here,  $m$  is the natural number closest to  $n - \frac{\delta}{\omega_z}$ , and I have defined:

$$\begin{aligned} \Omega_{n,m} &= -\frac{g_2^*g_1}{\Delta_R}\langle n|e^{i\Delta k_z\hat{z}}|m\rangle \\ &= -\frac{g_2^*g_1}{\Delta_R}\langle n|e^{i\eta(\hat{a}_z+\hat{a}_z^\dagger)}|m\rangle, \end{aligned} \quad (3.27)$$

where  $\eta_z \doteq \Delta k_z z_0$  is the Lamb-Dicke parameter for the two-photon transition and  $z_0 = \sqrt{\frac{\hbar}{2m\omega_z}}$  is the spread of the ground state harmonic oscillator wave function in  $z$ .

In general  $\eta_m = \Delta \mathbf{k} \cdot \hat{\mathbf{e}}_m m_0$  ( $m \in \{x, y, z\}$ ), where  $m_0$  is the spread of the ground state harmonic oscillator wave function in direction  $m$ .

Thus, according to Eq. (3.26), the dynamics induced by the two-photon, stimulated Raman transitions are qualitatively the same as those described in the last Section for a single laser beam, with the exceptions that  $\mathbf{k} \rightarrow \Delta \mathbf{k}$  and  $\omega_L \rightarrow \omega_1 - \omega_2$ . The advantage is that, for transitions between atomic levels separated by radio frequencies, we retain the frequency and phase control associated with rf, but at the same time achieve the high field gradients associated with optical transitions. We also achieve the benefit of being able to arrange  $\Delta \mathbf{k}$  so that we are sensitive to all directions of the ion's motion, only one direction of ion motion, or such that we are entirely insensitive to the ion's motion.

One possible issue with stimulated Raman transitions is that there will be some population in the “virtual” level  $|v\rangle$ , which decays with a time constant of 8 ns. We may make an estimate of the probability that the virtual level is populated in, for example, a  $\pi$ -pulse operation, by solving Eq. (3.22) for  $\tilde{C}_{3,\mathbf{n}}$ . Roughly speaking,  $|\tilde{C}_{3,\mathbf{n}}| \sim |\frac{g}{\Delta_R}|$ , where  $g$  is on the order of the single-photon coupling strengths  $g_1$  and  $g_2$ . However, from Eq. (3.27), we also have that the carrier Rabi frequency is roughly given by  $\Omega = \frac{g^2}{\Delta_R}$ , so that  $g \approx \sqrt{\Omega \Delta_R}$ . Thus,

$$\tilde{C}_{3,\mathbf{n}} \approx \sqrt{\frac{\Omega}{\Delta_R}} \quad (3.28)$$

$$P_v = |\tilde{C}_{3,\mathbf{n}}|^2 \approx \frac{\Omega}{\Delta_R}. \quad (3.29)$$

For typical operating conditions,  $\Omega/2\pi \approx 1$  MHz and  $\Delta_R/2\pi \approx 10$  GHz, so that  $P_v \approx 10^{-4}$  in a  $\pi$ -pulse operation. Decay from the virtual level is thus a small effect<sup>7</sup>.

---

<sup>7</sup> In principle, we would like to increase  $\Delta_R$  as much as possible in order to minimize the effects of decay from the virtual level. However, if  $\Delta_R$  is bigger than the  $2p \ ^2P$  fine-structure splitting ( $\approx 197$  GHz), destructive interference between the  $^2P_{1/2}$  and  $^2P_{3/2}$  virtual levels makes the stimulated-Raman coupling between  $|\downarrow\rangle$  and  $|\uparrow\rangle$  ineffective.

### 3.4 Spin Diagnostics: the Ramsey Experiment

One experiment which will appear in different forms throughout this thesis is the “Ramsey experiment” [95], which is typically used for high-precision spectroscopy. In the Ramsey method, a  $\frac{\pi}{2}$  pulse is applied to an atom or sample of atoms which previously has been prepared in some pure state. The state is then allowed to evolve without perturbation by applied fields for a time  $T_R$ , after which time a second  $\frac{\pi}{2}$  pulse is applied and the probability that the atom(s) remains in its initial state is probed. In the usual nomenclature, the first and second  $\pi/2$ -pulses are referred to as the first and second “Ramsey zones.” If the applied radiation is on resonance and the Ramsey zones have the same laser phase, then the probability of the atom remaining in the initial state is zero; for a general detuning from resonance, a series of narrow fringes is found as a function of the detuning. The Ramsey method offers an approximate factor of two improvement in resolution over the (optimum) Rabi flopping in spectroscopy, as well as offering practical advantages for atomic beam standards (in particular, for microwave spectroscopy) [95].

In our experiments, we typically build up spectra by keeping  $T_R$  fixed while sweeping the frequencies  $\nu_{pr}$  of the  $\pi/2$ -pulses. In order to determine  $P_{\downarrow}(\nu_{pr})$ , we may multiply the matrices corresponding to on-resonance  $\pi/2$ -pulses from Eq. (3.13), with a matrix  $\mathcal{M}_{fe}$  sandwiched in between to account for the effects of the free evolution during the time  $T_R$  between the  $\pi/2$ -pulses:

$$\mathcal{M}_{fe} = \begin{bmatrix} e^{-i\delta t/2} & 0 \\ 0 & e^{i\delta t/2} \end{bmatrix}. \quad (3.30)$$

This procedure is straightforward, but the expressions are complicated enough to obscure the underlying physics.

To obtain a clearer picture of the Ramsey experiment, consider instead the case in which the laser is on resonance with the  $|\downarrow\rangle \leftrightarrow |\uparrow\rangle$  transition, but where we sweep

the phase  $\phi$  of the second  $\pi/2$ -pulse. In this case, Eq. (3.13) becomes:

$$\begin{bmatrix} \frac{1}{\sqrt{2}} & \frac{-i}{\sqrt{2}}e^{i\phi_j} \\ \frac{-i}{\sqrt{2}}e^{-i\phi_j} & \frac{1}{\sqrt{2}} \end{bmatrix}, \quad (3.31)$$

where  $\phi_j$  ( $j = 1, 2$ ) is the phase of the  $j^{\text{th}}$  laser pulse. Taking  $\phi_1 = 0$  and  $\phi_2 = \phi$ , and multiplying the matrices together, we have <sup>8</sup> :

$$\frac{1}{2} \begin{bmatrix} 1 - e^{i\phi} & -i(1 + e^{-i\phi}) \\ -i(1 + e^{i\phi}) & 1 - ie^{-i\phi} \end{bmatrix}. \quad (3.32)$$

Thus, if we start out in the state  $|\downarrow\rangle$  and perform the experiment, the probability  $P_{\downarrow}(\phi)$  of finding the atom in  $|\downarrow\rangle$  at the completion of the second Ramsey zone is given by:

$$P_{\downarrow}(\phi) = \frac{1}{2}(1 - 2 \cos \phi) = \sin^2 \phi. \quad (3.33)$$

This describes sinusoidal oscillations in  $P_{\downarrow}$  as a function of the phase difference between the  $\pi/2$ -pulses. For small detunings of the laser from resonance, the predominant effect is due to the free evolution matrix, Eq. (3.30), which results in a net phase difference between the first and second Ramsey zones. Thus, Eq. (3.33) also applies to such cases.<sup>9</sup>

Fig. 3.5 shows typical Ramsey fringes, from an experiment in which the Ramsey zone pulse frequencies were varied near resonance.

### 3.5 Mapping Information From Motion to Spin

The interactions between the ion and the lasers couple the ion's spin and motional degrees of motion, through the field gradients of the laser. We may use this coupling to engineer the ion's quantum state of motion, as will be discussed in Ch. 6. Alternately,

---

<sup>8</sup> This equation is the same as that obtained in the case where the phase is held constant, but the detuning is changed — in the case that the detuning is small enough to ignore during the  $\pi/2$ -pulses, but where  $T_R$  is large enough that the detuning plays a large effect during the free evolution. This is easy enough to verify by using Eq. (3.31) for the  $\pi/2$ -pulses and Eq. (3.30) for the free evolution, and comparing the result to Eq. (3.32). Aside from an irrelevant overall phase factor, the two results are identical.

<sup>9</sup> For larger detunings, the complete result also exhibits an envelope which is given by the same line shape which would result from Rabi spectroscopy

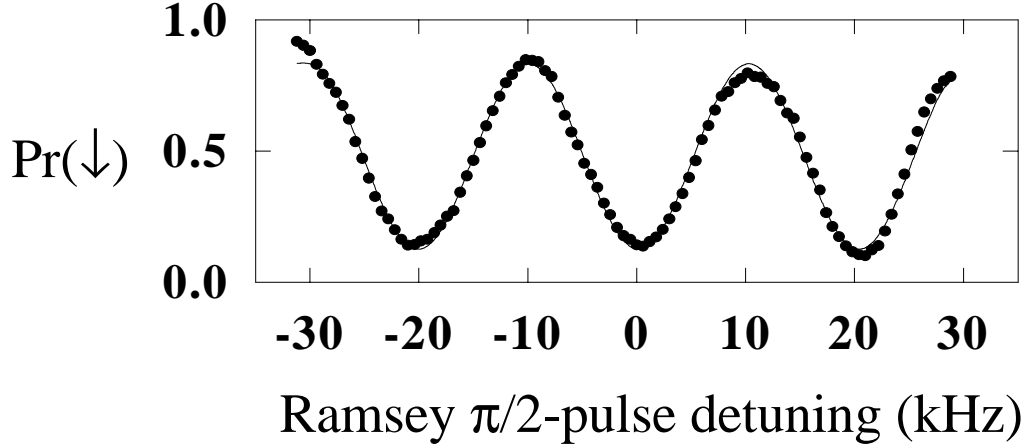


Figure 3.5: Ramsey fringes taken with an initial  $|\downarrow\rangle$  state. For these data, the frequencies of the Ramsey zones ( $\pi/2$ -pulses) were varied near the  $|\downarrow\rangle \leftrightarrow |\uparrow\rangle$  resonance frequency. For small detunings, the Ramsey fringes are well-fit by the sinusoidal form of Eq. (3.33).

we may use the coupling to map information about the ion’s motion onto its spin degree of freedom. This is necessary because we do not have the ability to measure the motional state occupation numbers directly. To do perform the mapping, we start with the ion in spin down and in some “unknown” (but reproducible) motional state:  $|\psi\rangle = |\downarrow\rangle \sum C_n |n\rangle$ . We then turn on the Raman beams, tuned to some particular motional sideband; in practice we choose to tune to the blue sideband.

If we leave the interaction on for a time  $t_{pr}$ , then measure the probability  $P_{\downarrow}$  that the ion is in  $|\downarrow\rangle$ , we find that

$$P_{\downarrow}(t_{pr}) = \sum P_n \cos^2(\Omega_{n,m} t_{pr}) = \frac{1}{2} \sum P_n (1 + \cos(2\Omega_{n,m} t_{pr})) \quad (3.34)$$

as discussed in Sec. 3.2 and indicated for a Fock state in Fig. 3.4(b). In Eq. (3.34),  $P_n = |C_n|^2$ . By performing a Fourier decomposition of the Rabi flopping curve, we can extract the  $P_n$ ’s. Furthermore, we can do this with *unit* quantum efficiency as long as the different Rabi frequencies  $\Omega_{n,m}$  are well-resolved. On the blue sideband, in

the Lamb-Dicke regime,  $\Omega_{n,n+1} = \eta\Omega\sqrt{n+1}$ , and so it is easy to resolve the different Fourier components.

In the experiment, background heating of the ion's motion and technical noise (laser beam intensity fluctuations, fluctuating background magnetic fields, etc.) wash out the Rabi flopping curves, as is evident in Fig. 3.4(b). To approximate these effects, we may write:

$$P_{\downarrow}(t_{pr}) = \frac{1}{2} \sum P_n (1 + \cos(2\Omega_{n,m}t_{pr})e^{-\gamma_n t_{pr}}) + \mathcal{B} \quad (3.35)$$

where  $\mathcal{B}$  is due to background counts and the  $\gamma_n$  are  $n$ -dependent decay coefficients.<sup>10</sup>

The data analysis proceeds as before except that a singular-valued decomposition analysis with decaying sinusoids as basis functions is used instead of Fourier analysis [96]. The frequencies of the various (decaying) sinusoidal basis functions are calculated from a base Rabi frequency (either the carrier or the  $|\downarrow, n=0\rangle \leftrightarrow |\uparrow, n=1\rangle$  transitions) using Eq. (3.12).

In summary, then, the interaction between the ion and the motion provides us with the “handle” we use to manipulate the ion's motion and also with the “camera” we use to analyze this motion.

---

<sup>10</sup> For example, if the decay is due to slow laser intensity fluctuations, then different Fock state flopping curves decay in the same number of flops and so, in a different absolute time.